

Water Resources Research®

RESEARCH ARTICLE

10.1029/2021WR031746

Markovian Models for Microplastic Transport in Open-Channel Flows

Liming Xing^{1,2} , Diogo Bolster² , Haifei Liu¹ , Thomas Sherman² ,
David H. Richter² , Kyle Rocha-Brownell², and Zhiming Ru¹ 

¹School of Environment, Beijing Normal University, Beijing, China, ²Department of Civil & Environmental Engineering & Earth Sciences, University of Notre Dame, Notre Dame, IN, USA

Key Points:

- Three Markov models with different degrees of correlation are implemented to model transport of microplastic particles in open channel flows
- Each model is tested on two datasets, one from a high-fidelity simulation, and the other from laboratory experiments
- Correlated models show advantages over the uncorrelated CTRW model in predicting breakthrough curves

Supporting Information:

Supporting Information may be found in the online version of this article.

Correspondence to:

H. Liu,
haifei.liu@bnu.edu.cn

Citation:

Xing, L., Bolster, D., Liu, H., Sherman, T., Richter, D. H., Rocha-Brownell, K., & Ru, Z. (2022). Markovian models for microplastic transport in open-channel flows. *Water Resources Research*, 58, e2021WR031746. <https://doi.org/10.1029/2021WR031746>

Received 6 DEC 2021

Accepted 29 JUL 2022

Author Contributions:

Conceptualization: Liming Xing, Diogo Bolster

Funding acquisition: Haifei Liu

Methodology: Liming Xing, Thomas Sherman, David H. Richter, Kyle Rocha-Brownell

Software: Liming Xing

Supervision: Haifei Liu

Validation: Liming Xing, Zhiming Ru

Writing – original draft: Liming Xing

Writing – review & editing: Diogo Bolster, Haifei Liu, David H. Richter

Abstract The ubiquity of microplastics in marine environments is of growing concern and is increasingly receiving widespread attention. Due to the role of rivers and streams as suppliers of microplastics to the marine environment, it is essential to accurately capture their movements at these scales, but modeling and experimental knowledge in such settings is still limited. In this work, three Markov models, including a continuous time random walk model, Bernoulli model, and spatial Markov model (SMM), are implemented to investigate polyethylene particles transport in open-channel flows. First, a three-dimensional high-resolution direct numerical simulation (DNS) fully resolves a canonical open-channel flow, and particle transport is simulated using idealized point particles. Then, a series of laboratory transport experiments are conducted in a circulating water tank, and particle image velocimetry methods are used to obtain particle-tracking data. We find that the correlated Bernoulli model and SMM can successfully reproduce the transport of both DNS and laboratory experiments, particularly in the prediction of measured breakthrough curves, which highlights the importance of correlation between the successive steps. A major benefit of these models is a computational cost that is several orders of magnitude less than, for example, DNS, which demonstrates their high-efficiency and effectiveness. Therefore, this research offers new insights into the transport of microplastics in open-channel systems like rivers and streams, which is necessary to prevent and reduce the environmental hazards of microplastics.

1. Introduction

Plastic is used extensively in products used in our daily lives due to attributes such as portability, flexibility, economy, toughness, and resistance to corrosion. However, some attributes, such as a long lifetime and persistence, can cause environmental issues, including adverse impacts on water systems. It has been estimated that between 4.8 and 12.7 million metric tons of plastic debris entered the marine ecosystem in 2010 (Jambeck et al., 2015). Much of this has or takes the form of plastic particles smaller than 5 mm in size—classified as microplastics (Arthur et al., 2008)—which are potentially toxic in an aquatic environment and a major concern of environmental researchers (Gong & Xie, 2020; Sighicelli et al., 2018; Zhang et al., 2017). Indeed, many studies have demonstrated microplastic detection in surface waters (Zhao et al., 2015), water columns (Nel & Froneman, 2015), and surrounding sediments (Browne et al., 2011). In particular, flows in riverine systems are an important pathway for microplastic pollution (Murphy et al., 2016), which can persist for decades due to plastics' natural longevity, and other hazardous substances (e.g., heavy metals, organic pollutants) can be released during the aging of plastic debris (Koelmans et al., 2014). Furthermore, other toxins and pollutants can be absorbed by microplastics, which act as carriers to enable transport over much longer distances than in their absence (Guo et al., 2012; Hüffer & Hofmann, 2016). Physical properties, such as density or shape, of microplastics detected in water may vary significantly depending on the category of polymer and duration of its exposure in the environment (Khatmullina & Isachenko, 2017). These properties play an important role on how microplastics interact with the flow (e.g., buoyancy, drag) (Xuan & Jwa, 2019). As an important example, polyethylene (PE, $\rho_p = 0.956 \text{ kg/m}^3$) in many forms is widely used in the manufacturing of film, packaging materials, containers and other common uses. In recent years, PE has become the largest category of the total plastic production, accounting for 36% (Geyer et al., 2017). PE particles extensively exist in water ways and migration through surface waters has been determined to be significant (Teng et al., 2020). While generally microplastics can come in various shapes, the dominant shape of PE particles is as a roughly spherical or cylindrical piece of plastic debris (Li et al., 2021), shown as Figure 1.



Figure 1. Image taken with stereo microscope of PE (polyethylene).

A key challenge in addressing the environmental concerns is to understand how microplastics move, and their pathways in hydrologic systems. Techniques to detect microplastics in natural systems are still in the early stages of development (Löder et al., 2015). A central challenge is understanding and modeling the fundamental physical behaviors of microplastic particles in flowing systems, given that particles range in size, shape, density, and buoyancy (Dibenedetto & Ouellette, 2018). It is ultimately desired to make predictions over large scales (e.g., rivers and streams). In modeling to predict the movement of microplastics in water, a major gap exists in understanding transport in river-like settings (i.e., an open-channel flow), where turbulence effects interact with the physical properties of the plastics. While microplastics are predominantly thought of as a threat to oceans, rivers are probably the major source of plastic debris (Besseling et al., 2017; Mughini-Gras et al., 2021; Wang et al., 2020). Therefore, to understand transport in these settings is critical, and knowledge of the physical transport mechanisms in open-channel systems is the basis for the understanding of microplastics in aquatic environments. Vincent and Hoellein (2021) adapted nutrient spiraling metrics, a group of calculations that quantify particle movement, to describe microplastic transport in urban streams. Besseling et al. (2017) used the NanoDUFLOW model to investigate the fate of microplastics in riverine systems. However, to date, models for simulating microplastic particle transport in natural rivers are still in their infancy. One reason is a paucity of experiments to validate them. Additionally, there are a broad range of spatiotemporal scales in stream and river systems, where hydrodynamic processes and pollutant transport are very complicated. Not only that, mobility of microplastics in water environments may also be complicated by processes such as mechanical filtration, electrical surface interactions, fiber self-agglomeration (flocculation), and trapping (Engdahl, 2018). All of these make developing rigorous transport models for microplastics challenging and there is a need to develop powerful, cost-efficient models to investigate the transport of microplastic particles in river systems. Additionally there is a need to conduct benchmark laboratory studies to enrich the knowledge base and guide the accuracy and reliability of proposed models.

The continuous time random walk (CTRW) model has been very successful across a range of hydrologic systems (Berkowitz et al., 2006), including surface water systems (Aubeneau et al., 2014). While immensely powerful, like all models these are based on assumptions relating to independence and correlation, which restricts the scales at which they are valid. Recent variants have incorporated correlation via a Markov chain and shown success at scales where previous iterations were not valid (Aquino & Borgne, 2021; Bolster et al., 2014; Kang et al., 2014, 2015; Le Borgne et al., 2008a, 2011; Sherman et al., 2020). Applications in surface flows have been limited, with the exceptions of modeling an entire watershed (Engdahl & Bolster, 2020) and exchange between surface and subsurface (Kang et al., 2019; Sherman et al., 2019). These models have seen success in studying the transport of particulates in the atmospheric boundary layer (Park et al., 2020), which, from a fluid mechanics perspective, resembles an open-channel flow in several ways. Classical CTRW models describe transport by

conceptualizing the solute as a large number of discrete particles that transit in time and space by probabilistically sampling from a time/distance distribution at each step,

$$x_i^{n+1} = x_i^n + \Delta x_i^n, \quad t_i^{n+1} = t_i^n + \Delta t_i^n, \quad (1)$$

where both the spatial increments Δx_i^n and temporal increments Δt_i^n of particle i at step n are random. In some applications, transition distances and travel times are randomly sampled from a distribution (Le Borgne et al., 2008a); in others, one type of increment is fixed and the other is random (Le Borgne et al., 2008b); and in still others, both are random in a coupled or uncoupled manner (Sherman et al., 2019). CTRW models capture physical features from smaller scales in an upscaled framework, and accurately describe large-scale transport with high efficiency. Classical CTRW models assume particles jump between steps fully independently, while successive steps in Markov models are correlated, a feature which has been shown to be key in capturing certain features, such as persistent early- and late-time arrivals (Le Borgne et al., 2011), non-monotonic breakthrough curves (BTCs) (Bolster et al., 2014), and intermittency effects (De Anna et al., 2013; Holzner et al., 2015; Morales et al., 2017), which are common in many flows. Correlation is included in such a Markov model in many ways, such as through transition matrices (Le Borgne et al., 2008a), Bernoulli trial models (Holzner et al., 2015), and Orstein-Uhlenbeck models (Morales et al., 2017).

Key to these models are transition time distributions, which in practice are often found via BTCs which are concentration time series at some distance downstream from a release point. By measuring BTCs at multiple downstream locations, correlation effects can be estimated either by direct measurement or inverse modeling. Most previous studies have measured BTCs by tracking a large number of particle trajectories from high-resolution numerical simulations (Le Borgne et al., 2011; Sherman et al., 2019, 2020), which is somewhat impractical in real systems. Kang et al. (2015) were first to apply the SMM to field observations, accounting for both velocity distributions and correlations. Holzner et al. (2015) and Morales et al. (2017) conducted laboratory experiments using particle tracking velocimetry, and used information from particle trajectories in their correlated CTRW models. Sherman et al. (2018) developed an inverse method to calculate transition matrices from laboratory tracer experiments.

In this study, for the first time, CTRW models are extended to simulate the transport of real PE microplastic particles in open-channel flows. We apply and test three CTRW models with different degrees of correlation to model the transport of microplastic particles in an open-channel water flow. All three are CTRW/Markov models. We refer to them collectively as such, but individually as the CTRW, Bernoulli, and spatial Markov models. Each model is tested on two datasets, one from a three-dimensional (3D) high-resolution direct numerical simulation (DNS), and the other from laboratory experiments that track several real microplastic particles in a flume. From this, we aim to answer the following questions: “Do Markovian models faithfully capture PE particle transport in an open-channel flow?” and “Are correlation effects between successive steps important in such settings?”

2. Methods

Microplastic transport is studied in open-channel flows using both numerical simulations and laboratory experiments, and from these, we develop multiple upscaled random walk models. In the first case, a 3D high-fidelity DNS is performed to represent transport in an ideal open-channel system whose flow details are known completely. In the second case, laboratory experiments are conducted in a straight water tank with real microplastic particles, where the physical properties of flows and statistical data of particles are measured and collected. The CTRW, Bernoulli, and spatial Markov models are used to reproduce BTCs from both the laboratory experiments and DNS simulations. We begin by describing the DNS setup and laboratory experiments.

2.1. DNS Framework

A 3D DNS coupled with Lagrangian tracers is utilized in an ideal open-channel flow system to simulate the transport of microplastics. The DNS code is well-established and has been validated and tested for grid convergence (Richter & Sullivan, 2013; Sherman et al., 2019), and we use a similar domain setup, without the effects of subsurface flow. The governing equations in the DNS are the Navier-Stokes equations for incompressible fluid mass and momentum conservation, which can be written as

$$\nabla \cdot \mathbf{u} = 0, \quad (2)$$

$$\frac{\partial \mathbf{u}}{\partial t} + \mathbf{u} \cdot \nabla \mathbf{u} = -\frac{1}{\rho} \nabla p + \nu \nabla^2 \mathbf{u}, \quad (3)$$

where \mathbf{u} is the velocity vector in the x , y , and z directions; p is pressure; t is time; ν is the kinematic viscosity of the fluid; and ρ is fluid density.

The flow solver uses pseudospectral discretization in the homogeneous x and y directions, and second-order finite differences in the z direction. A computational mesh of $[N_x, N_y, N_z] = [128, 128, 128]$ is divided over a domain size of $[L_x, L_y, L_z] = [2H, H, H]$, where $H = 0.3$ m is the water depth. Grids are generated uniformly in the x and y directions, while grid stretching is used in the vertical direction; Δz near $z = 0$ and $z = H$ is reduced to accurately resolve the motions at the lower and upper surfaces. At the top boundary, $z = H$, a no-stress boundary condition is used, and on the lower boundary, $z = 0$, a no-slip condition is imposed. The lateral boundaries in x and y are periodic (Figure 2). A fixed pressure gradient is used to drive flow in the x direction, and a fixed time step of $\Delta t = 0.002$ s is applied in simulations. Statistically stationary conditions are obtained by letting the turbulence spin up before releasing microplastic particles, and the simulations are spun up for 8×10^5 time steps to develop stationary flow fields before releasing particles.

The Eulerian velocity fields generated by the DNS are used to transport Lagrangian particles. PE particles are released at the same time at a specified location of $x_{t=0} = [0, \gamma, H - d_a/2]$, where d_a is the particle diameter (see Section 2.2.1) and γ is a uniformly distributed random number spanning the full length along the y direction. In terms of the buoyancy of the PE particles, the gravitational acceleration of the PE particles is defined as $g(1 - \rho/\rho_p)$, where $g = 9.8$ m/s² represents the gravitational acceleration on the earth. At the upper and lower boundaries, the particles are elastically reflected, constituting a no-flux condition from a Lagrangian point of view, that is, when a particle crosses the top boundary with position $(x, y, z + \Delta z)$ it is re-positioned into the computational domain at $(x, y, z - \Delta z)$. The particles experience the same periodic lateral boundaries as the fluid velocity. The total number of particles is set to $N_p = 10^6$, and the simulations are run for 1×10^5 time steps after the particles are initiated into the spin-up, turbulent velocity field.

In the Markov framework, particle trajectories can be sampled from a joint travel distance and time distribution, and the trajectories are governed by Equation 1. If the spatial increment is fixed $\Delta x_i^n = \Delta x$, then the temporal increments Δt_i^n should be sampled from a distribution of travel times, which can be estimated by measuring the first passage time distribution of particles arriving at $x = x_0 + \Delta x$, where x_0 is the initial location of the particles. In DNS modeling, x_p^i ($1 \leq i \leq N_p$) denotes a recorded trajectory of a particle during the simulation, which allows us collect the arrival time t_i^n when particle i passes specified location $n\Delta x$ during the transport process. Considering a stable and fully mixed case, we choose the locations as the points between $100\Delta x$ and $104\Delta x$, corresponding to arrival times at locations t_i^{100} to t_i^{104} . We define normalized arrival times $t_i^1 = t_i^{101} - t_i^{100}$, $t_i^2 = t_i^{102} - t_i^{100}$, $t_i^3 = t_i^{103} - t_i^{100}$, and $t_i^4 = t_i^{104} - t_i^{100}$, which represent the times for a particle to go from the first to last spatial checkpoint. In this study, $\Delta x = 0.096$ m. If we divide the particle arrival times into m classes of equal probability, t^j ($1 \leq j \leq m$), then a temporal interval $[t^j, t^{j+1}]$ can be used to count the number of particles in the interval, and these numbers at fixed locations are BTCs.

2.2. Flume Experiments

2.2.1. Microplastic Particles

PE particles used in the flume experiments and purchased from Dushanzi Petrochemical Company (Xinjiang, China). A stereo microscope (XT-03C/03B, PUZHE Photoelectric Instrument Co., Ltd., China) with a microparticle size analysis system (UV-G) was used to determine individual particle sizes. As the particles were not of perfect-spherical shape (Figure 1), an equivalent spherical diameter (d_e) was introduced (Dietrich, 1982). This was calculated based on a best-fit ellipse method (Kumar et al., 2010) using measured major (a), minor (b), and intermediate (c) axes, where $d_e = \sqrt[3]{abc}$ (Kowalski et al., 2016). Measuring 20 randomly selected particles, d_e varied between 3.93 and 4.80 mm, with an average of $d_a = 4.28$ mm.

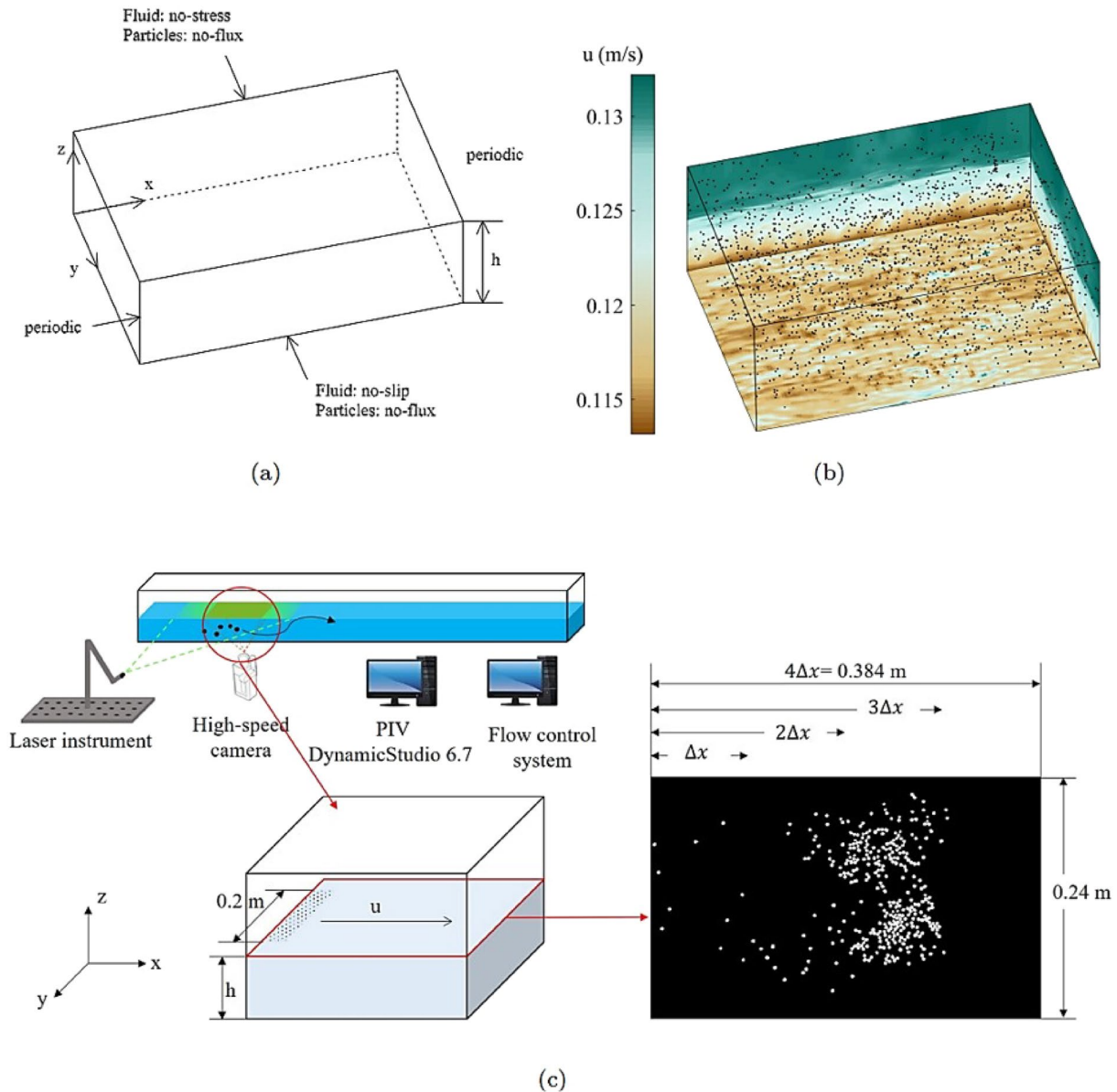


Figure 2. Schematic diagrams of open-channel flows in an idealized direct numerical simulation (DNS) and a real-world setting: (a) boundary conditions within DNS domain; (b) instantaneous state of 3D DNS at 1×10^5 time steps, where color contours indicate velocity magnitude and black dots are particles moving in the open-channel flows; (c) experimental setup and successive steps in Markov framework.

2.2.2. Experimental Procedure

Flume experiments were conducted in an open circulating water tank with a flow-control system. Implementation included a laser, high-speed camera, operational software, and imaging platform (DynamicStudio 6.7, Figure 2c). The camera was calibrated to get sharp images over a field of view 0.384 m long and 0.240 m wide. In the experiments, three cases with water depth of 0.290 m were considered, corresponding to velocity conditions set by the flow-control system. Once a stable flow was obtained, the DynamicStudio acquisition module was set up (time between pulses, trigger rate, and number of images), and the laser was started and directed at the free water surface. A pulse of PE particles was released along the y axis, spanning a width of 0.200 m. A filter was mounted on the camera lens to protect the optical sensors from the laser. Flow parameters and experimental settings are shown in Table 1, where the selected flow velocities indicate the Froude number in this paper ranges from 0.08 to 0.15, and effective particle number stands for the number of particles which can be captured by the camera for processing with particle-tracking. Each case was repeated for three trials.

Table 1
Experimental Specifications and Three Cases

Items	Detail	
Channel dimensions	0.8 × 0.8 × 25.0 m	
Laser instrument	Mode	Double frame
	Intensity	6
High-speed camera	Range	0.384 × 0.240 m
	Focal length	3.1
	Aperture size	5.6
	Filter	532 mm
DynamicStudio	Time between pulses	1364.25 μs
	Trigger rate	15 Hz
	Number of images	100
Case	Flow velocity (<i>u</i> , m/s)	Effective particle number
1	0.125	456
2	0.200	570
3	0.250	350

Similar to the data processing for the DNS, the spatial increment is a fixed Δx and temporal increments Δt_i^n should be sampled from a distribution of travel times, which can be estimated by measuring the first passage time distribution of particles arriving at Δx . After running all of the cases, the DynamicStudio database module processed and extracted images obtained from the high-speed camera, and the domain was divided into 59×37 subdomains during data processing. These images were imported into MATLAB and used to track the individual particles. Given particle-tracking data, we can collect arrival times of a particle t_i^n at specified downstream locations Δx , $2\Delta x$, $3\Delta x$ and $4\Delta x$ (subfigure on the right in Figure 2c), representing the times for a particle to go from the first to last spatial checkpoint.

2.3. Markov Models

2.3.1. CTRW Model

In a CTRW framework, particle trajectories can be sampled from a joint travel distance and time distribution $\psi(x, t)$. A particle's trajectory through time and space is governed by the Langevin equation, shown as Equation 1. As noted above, we take Δx_i^n to be a constant Δx , such that $\psi(x, t) = \psi(t) \delta(x - \Delta x)$ (Le Borgne et al., 2008a). Therefore, during the n th step, particle i jumps a distance Δx with a travel time Δt_i^n , randomly sampled from the time distribution $\psi(t)$, which can be estimated by measuring the first passage time

distribution of particles arriving at $x = x_0 + \Delta x$, where x_0 is the initial location of the particles. In our case, the time distribution $\psi(t)$ is the distribution of t_i^1 measured in the DNS and experiments. For Markov model studies, BTCs are a very standard metric for model testing in the transport literature; therefore, predicted BTCs from the CTRW model at the second, third, and final locations are used to compare predictions with DNS and experimental measurements.

2.3.2. Bernoulli Model

It has been documented in several hydrologic settings that strong velocity correlation properties may exist (i.e., fast particles persist at being fast, and slow particles at being slow), which may affect large-scale transport behavior (Le Borgne et al., 2008a; Park et al., 2020; Sherman et al., 2020). We propose a highly parsimonious model that aims to account for such correlation. Again, particles move through time and space by random walk (Equation 1), but a correlation is imposed on successive jumps by a Bernoulli process such that

$$t_i^{n+1} = \begin{cases} t_i^n, & p, \\ \Delta t_i^n, & 1 - p, \end{cases} \quad (4)$$

where Δt_i^n randomly sampled from the distribution $\psi(t)$, which is as same as the $\psi(t)$ in the CTRW model; p is determined as the probability of persisting in a state over a distance Δx . In other words, a particle will persist with the same transition time with probability p and switch transition time with probability $1 - p$, where p can vary from 0 to 1. Thus particles have a finite probability of persisting at the same speed as in the previous transition. The Bernoulli model reduces to the CTRW model when $p = 0$, while $p = 1$ corresponds to perfect persistence and ballistic motion (i.e., all particles always move at the same speed). Therefore, we ran a full range of values of p between 0.1 and 0.9 for the Bernoulli model to determine the optimal p . Similar to the CTRW model, BTCs from the Bernoulli model can be compared with the DNS and experimental measurements.

2.3.3. SMM

The governing equations for the SMM can also be written as Equation 1. However, a key characteristic of the SMM is that travel times of successive steps can be correlated, as with the Bernoulli model. A key difference is that the SMM tries to characterize these correlations more broadly, and a conditional probability density $r(\Delta t/\Delta t')$

is used to do so. $r(\Delta t|\Delta t')$ characterizes the probability that a particle has a time increment of Δt , given it had one of $\Delta t'$ during the previous time step. From a practical standpoint, it is convenient to represent $r(\Delta t|\Delta t')$ discretely as a transition matrix (Le Borgne et al., 2008a).

We divide the travel time distribution $\psi(t)$ into k classes of equal probability with C_i ($1 \leq i \leq k$). It should be noted here that the $\psi(t)$ in SMM is also as same as that in CTRW model and Bernoulli model because they were measured from the same data. A particle is contained in bin C_i if its transition time is in the range $\Delta t_i \leq \Delta t < \Delta t_{i+1}$. The fastest travel times are in bin C_1 , and the slowest are in bin C_k . Therefore, $r(\Delta t|\Delta t')$ can be discretized into a transition matrix as

$$T_{i,j} = \frac{\int_{\Delta t_j}^{\Delta t_{j+1}} \int_{\Delta t_i}^{\Delta t_{i+1}} r(t|t') \psi(t') dt' dt}{\int_{\Delta t_i}^{\Delta t_{i+1}} \psi(t) dt}, \quad (5)$$

where $T_{i,j}$ is the probability that a particle has a travel time in class j during step $n + 1$, given that it had a travel time in class i during step n . In this study, $k = 10$, which has been shown to be sufficient to obtain correlated effects and generate reliable results (Le Borgne et al., 2011). Therefore, the arrival times of the first two steps will be inputs for the SMM.

3. Results and Discussion

3.1. Markov Models and Idealized DNS

For the idealized open-channel system simulated in the DNS, the three Markov models were tested by comparing their ability to predict downstream transport by BTCs measured at multiple locations, given by $x = 102\Delta x$, $103\Delta x$, and $104\Delta x$. We tested these models using the DNS simulations as the reference. A mean absolute percent error (MAPE) was calculated between DNS simulations and model predictions as

$$MAPE = \frac{1}{m} \sum_{j=1}^m \left| \frac{N(t^j)_{DNS} - N(t^j)_{Mod}}{N(t^j)_{DNS}} \right| \times 100\%. \quad (6)$$

where $N(t^j)_{DNS}$ represents DNS simulations of the particle number at each discrete time and $N(t^j)_{Mod}$ represents model BTCs predictions including CTRW, Bernoulli, and SMM models; m represents the number of discrete particle arrival time intervals.

3.1.1. Correlation Parameterization

For both the Bernoulli and SMM models, we must parameterize correlation effects (i.e., choose a value of p for the Bernoulli model and define a transition matrix for the SMM model).

For the Bernoulli model, we calculated the MAPE between DNS simulations and the predicted BTC at $2\Delta x$ using values of p varying from 0.1 to 0.9 (see Figure S1 in Supporting Information S1); recall that for $p = 0$, the model collapses to the CTRW model, and $p = 1$ implies ballistic motion. We found the optimal to be $p = 0.9$, which corresponds to the minimum MAPE and suggests strong correlation.

Figure 3a displays the discrete transition matrix required for application of the SMM. Based on Equation 5, the x and y axes represent the classes of particles' travel times during step $n + 1$ and n , respectively, and the z axis (color scale) represents the probability of each cell. There is an obvious diagonal tendency, reflecting strong correlation in the considered system. This is consistent with the optimal value of $p = 0.9$ for the Bernoulli model. To quantify the degree of correlation, a correlation coefficient can be calculated as (Bolster et al., 2014),

$$CC = \frac{1}{k} \sum_{i=1}^k \sum_{j=1}^k T_{i,j}^2, \quad (7)$$

where CC can vary from $\frac{1}{k} \leq CC \leq 1$. $CC = \frac{1}{k}$ means there is no correlation between successive time steps, and T_{ij} represents a matrix whose elements are identical; $CC = 1$ means the transport is perfectly correlated and the diagonal elements are $T_{i,i} = 1$. The correlation coefficient in the case of the idealized DNS is $CC = 0.7804$, which indicates a relatively high degree of correlation between successive steps.

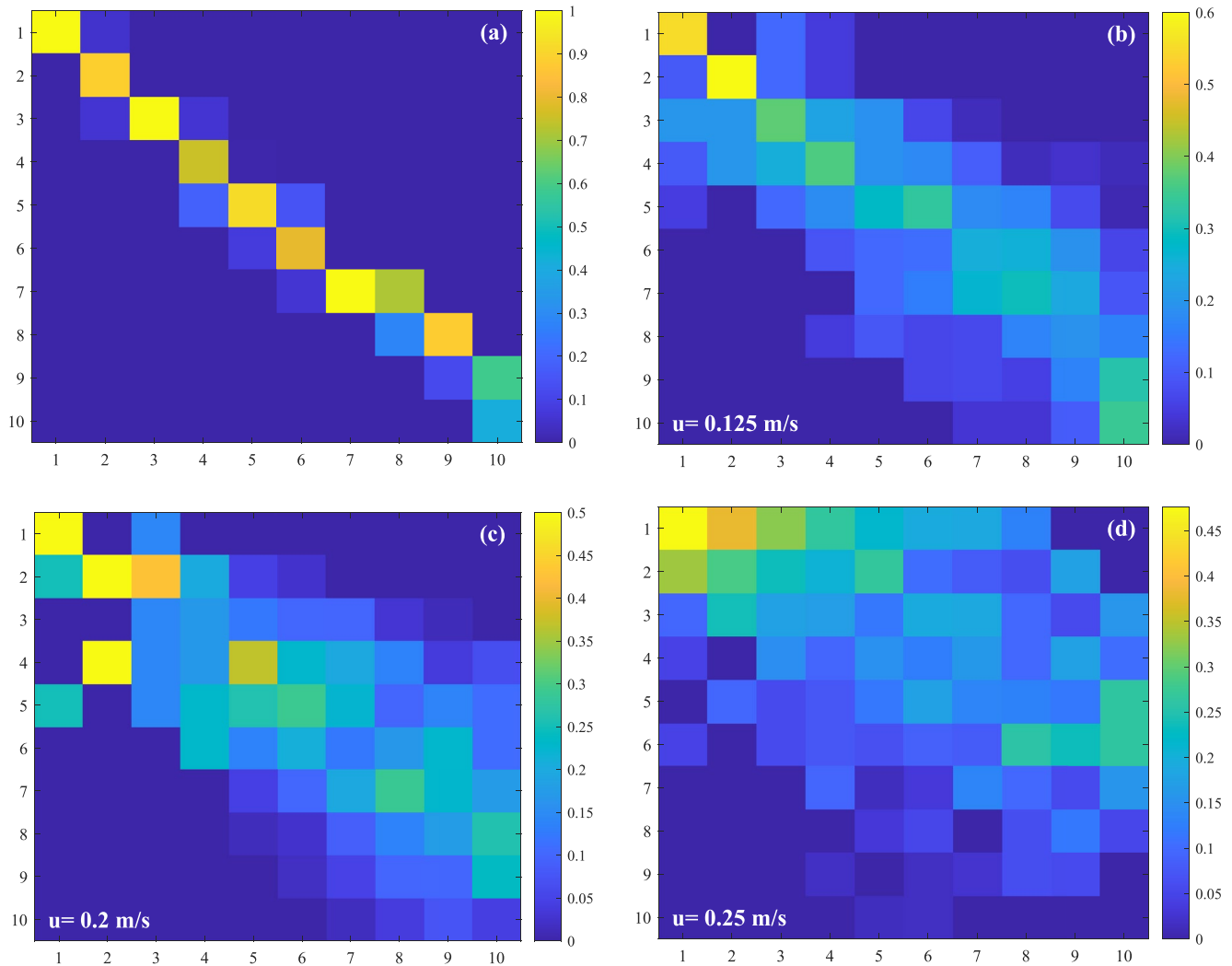


Figure 3. Transition matrices in spatial Markov model (SMM): (a) idealized DNS modeling; (b–d) three cases with different flow velocities in laboratory experiments.

3.1.2. Intermodel Comparison

We test the three Markov models, and compare the predicted BTCs and DNS modeling in Figures 4a–4c. Figure 4a shows that the CTRW model without considering correlation between successive steps cannot well capture the transport, especially the tails. Figure 4b shows the modeled BTCs of the Bernoulli model, which are generally in excellent agreement with the DNS results, for the tails as well as the peak location. For the SMM (Figure 4c), predicted BTCs match DNS results better than the CTRW model, but the SMM struggles to reproduce the tails.

The MAPE of all three models were also calculated (Table 2), and consistent with what we see in Figure 4b, the Bernoulli model exhibits the best accuracy at reproducing the DNS BTC results. The MAPE at all downstream locations is less than 7%. The high MAPE of CTRW highlights the importance of the correlation between successive steps. Therefore, comparing the three models to an idealized DNS simulation, the correlated Bernoulli model appears effective at capturing the physical properties of microplastics in a computationally efficient manner.

While the poorer performance of the CTRW model implies that correlation between successive steps is significantly important, the question remains as to why the SMM does not perform as well as the Bernoulli model. We speculate that the problem may relate to the enormously strong correlation effects in this case, relative to most previously studied situations, with one exception (Bolster et al., 2014). This may mean that only having 10 bins may not sufficiently resolve the full correlation structure. With the SMM, there is always a compromise between the number of bins and the amount of data required to accurately parameterize it. As the number of bins increases,

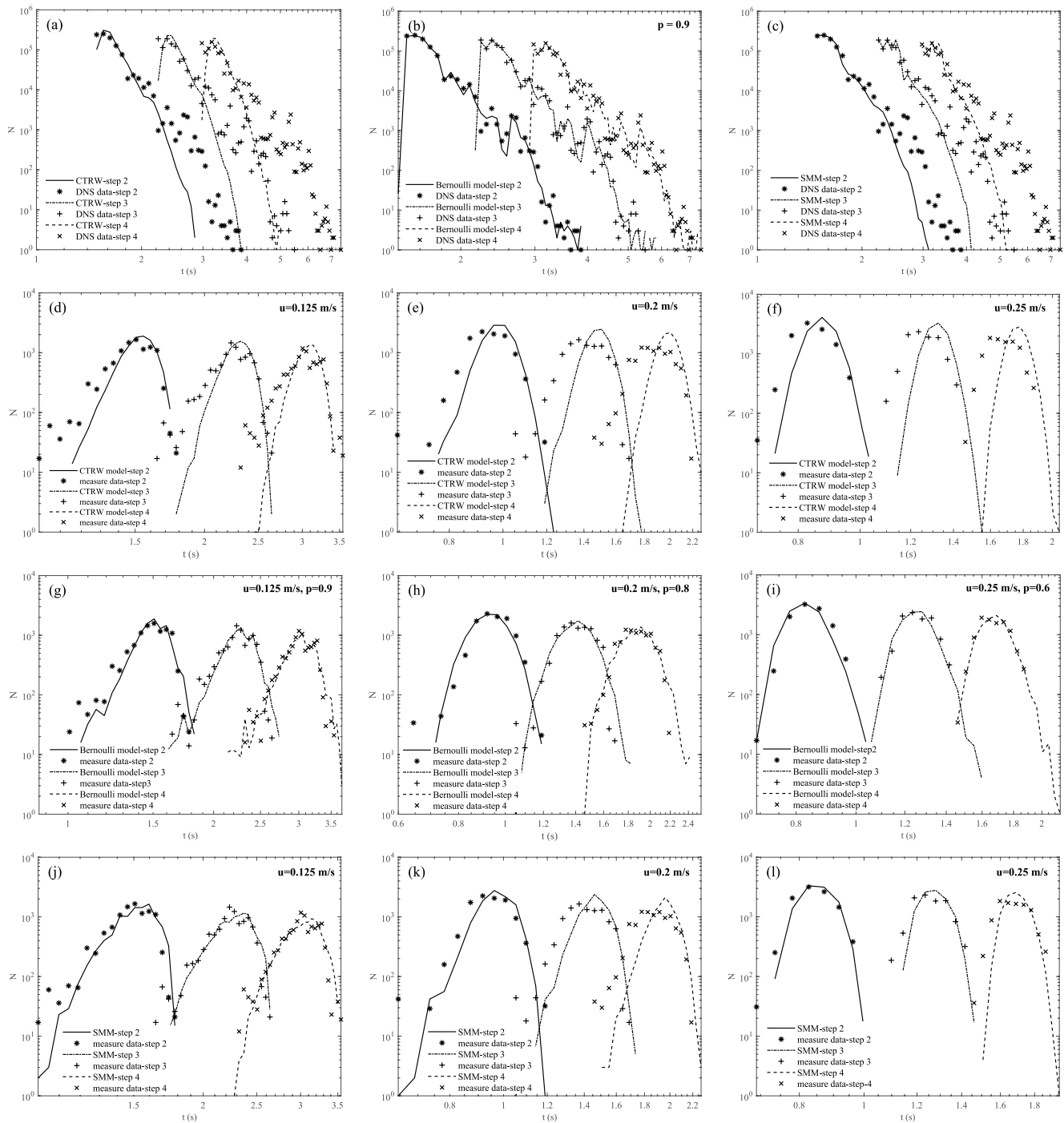


Figure 4. Predicted BTCs of three Markov models: (a–c) DNS modeling; (d–l) measurements under three cases with different flow velocities.

significantly more particles are needed to have a well-defined transition matrix that is not noisy, and to increase the number of bins with the number of particles we have here is simply infeasible. Indeed, a common criticism of the SMM is that the amount of detailed data required can be prohibitively large in many realistic settings (Sherman et al., 2020). Additionally, the Bernoulli model is the more parsimonious of the two, so its winning may actually be regarded as a positive outcome.

Table 2
MAPE Among the Three Models (Bernoulli With $p = 0.9$), Relative to DNS Simulations

Step	2	3	4
CTRW	0.490	0.686	0.823
Bernoulli model	0.042	0.065	0.062
SMM	0.314	0.161	0.139

3.2. Markov Models in Laboratory Experiments

Data processing of the experimental images produces particle-tracking results that allow comparison between measurements and model-predicted BTCs at steps 2, 3, and 4, corresponding to locations $x = 2\Delta x$, $3\Delta x$, and $4\Delta x$, respectively (Figure 2c). Similarly, MAPE can be calculated between measured data and model predictions.

3.2.1. CTRW Model

Figures 4d–4f compare BTCs predicted with the CTRW model and measured data for the three experimental flow velocities. These demonstrate that the CTRW model can provide a relatively correct trend of the BTCs, but cannot exactly predict them as compared to measurements. There are mismatches in predictions of early and late arrivals, especially for $u = 0.125$ m/s. The CTRW model predicts BTCs later than the measurements, especially for $u = 0.2$ and 0.25 m/s. Table 3 shows MAPE of the CTRW model. MAPE increases with downstream distance, compounding over time/space, likely compromising even further downstream predictability. This demonstrates that the CTRW model has difficulty capturing the full details of BTCs when directly sampling from the time probability distribution functions (PDFs) $\psi(t)$ without considering velocity correlations.

3.2.2. Bernoulli Model

As discussed above, the choice of probability p is critical for the Bernoulli model. To acquire the optimal p , we repeat the process, as done for the DNS results (see Figure S2 in Supporting Information S1). In this case, we find that the optimal p is not the same across the flow velocities, and is 0.9, 0.8, 0.6 for $u = 0.125, 0.2, 0.25$ m/s, respectively. Therefore, the correlation between successive steps becomes less important as flow velocity increases, as might be expected. Figures 4g–4i show the predicted BTCs of the Bernoulli model for all velocities with the respective optimal p , and compares them to measured data. The Bernoulli model can more accurately predict the early, peak, and late arrivals than the CTRW model (Figures 4d–4f). Focusing on $u = 0.125$ m/s, for instance, the model can reproduce the experimental measurements remarkably well in capturing the peak of every single BTC; however, the Bernoulli model predicts BTCs slightly later than the measurements (Figure 4g). MAPE is less than 10% in almost all runs with the Bernoulli model (Table 3), which indicates that the model can reliably generate accurate BTC predictions at all velocities. This again emphasizes the importance of correlation between successive steps, which should be seriously considered in this sort of transport environment.

3.2.3. SMM

The SMM requires a higher degree of parameterization due to the transition matrices, and for all experimental flow velocities, the transition matrices exhibit relatively strong diagonal trends (from top-left to bottom-right), indicating that the velocity correlation is significant (Figures 3b–3d). Comparing the correlation coefficient among three flow velocities $CC_{0.125} = 0.2514 > CC_{0.2} = 0.2482 > CC_{0.25} = 0.1999$, we found that the transition matrices corresponding to the lower flow velocities generally exhibit a stronger correlation, which also agrees with the observations from the Bernoulli model. Figures 4j–4l compare predicted and measured BTCs for the SMM. There are discrepancies at early times, and deviations increase with downstream distance. Compared to the Bernoulli model, the SMM excels at capturing late-time tails. However, Table 3 compares the Bernoulli model and the SMM using the MAPE metric, which demonstrates that SMM excels over Bernoulli model at a lower flow velocity, whereas the SMM performs less well compared to the Bernoulli model with an increasing

Table 3
MAPE Among Three Models (Bernoulli Model Calculated With Optimal p)

Step	0.125			0.2			0.25		
	2	3	4	2	3	4	2	3	4
CTRW	0.182	0.585	0.622	0.164	0.306	0.415	0.103	0.394	0.434
Bernoulli	0.133	0.095	0.095	0.055	0.093	0.056	0.053	0.044	0.022
SMM	0.090	0.063	0.057	0.089	0.167	0.151	0.064	0.080	0.053

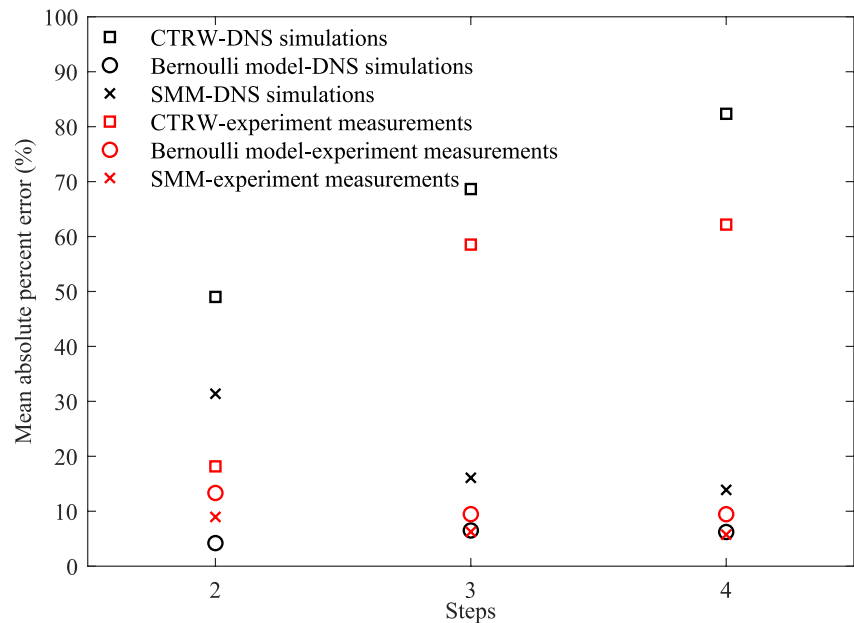


Figure 5. Mean absolute percent error (MAPE) between predicted breakthrough curves (BTCs) and observations (measurements of laboratory experiments when $u = 0.125$ m/s (red) and simulations of DNS modeling (black)).

flow velocity. In spite of this, unlike the DNS example, the SMM appears to sufficiently resolve the correlation structure with only 10 bins, most likely due to weaker correlation effects.

3.3. Model Comparisons and Benefits

To summarize the above results, MAPE between predicted BTCs and observations of laboratory experiments ($u = 0.125$ m/s) and DNS simulations are plotted (Figure 5). The large MAPE for the CTRW highlights the importance of correlation in the transport of microplastics in open-channel flow, regardless of whether it is the idealized DNS or a physical experiment. The Bernoulli model comes out on top in the ideal open-channel system of the DNS (black circles), and the SMM can capture the underlying physics of microplastic transport in the laboratory setting when $u = 0.125$ m/s (red crosses). Moreover, MAPE for both correlated models declines with distance, that is, the accuracy of the correlated Markov models improves as the transport distance increases.

In terms of computational expense, the three Markov models have a significant advantage over something like a DNS, as they do not need to resolve all scales of turbulent motion. We roughly calculate the required computational cost using CPU time, which is estimated as the product of the total time to run a simulation and the number of processors. In this work, the DNS with 10^6 microplastic particles costs $\mathcal{O}(10^6)$ CPU seconds, taking days to run on 64 Intel Ivy Bridge computational cores. The correlated Markov models, by contrast, take $\mathcal{O}(10^{-1})$ CPU seconds to complete a BTC prediction. This huge reduction illustrates a great advantage of the Markov models, but estimating model inputs without higher-fidelity particle-tracking simulations (such as DNS) is still an unsolved problem, hence, a full reduction in computational cost has not yet been truly achieved. At the same time, we implement the Markov models using model inputs from experimental measurements. As a result, the Bernoulli model and SMM can be parameterized and accurately predict BTCs, which can improve the reliability and practicality of the Markov models in the real world.

3.4. Model Limitations and Implications for Further Efforts

In reality, weathering and the material properties of microplastics including density, size, and shape, factors not considered explicitly in this study (Duan et al., 2021), will affect their behaviors in waterways. Therefore, future efforts should consider more detailed forms of the microplastics, so as to fully and comprehensively investigate

their transport in water. However, the results of this study provide new insights into the modeling of microplastic transport in highly dynamic streams and rivers, and would hopefully guide future efforts including, but not limited to:

3.4.1. Generalization

In this study, we applied Markov models in both an idealized and realistic open-channel system, and found good agreement between predictions and measurements from experiments/simulations. Given recent extensions to complex two- and three-dimensional systems in other settings such as transport through porous media, we speculate that it may be possible to extend the use of Markov models to other more complex flows, such as for example, coastal ones (Bianchi Janetti et al., 2020).

3.4.2. Combined Environmental Pollution and Ecological Impacts

As a long-distance transport carrier, microplastics, absorbing chemical contaminants (i.e., antibiotics, heavy metal), will lead to more complex coupled environmental pollution. The predicted results of microplastic transport from Markov models should be coupled to adsorption models as a basis to couple microplastic transport and associated contaminants. In addition, studies show that microplastics can be ingested by a range of aquatic organisms and can even be incorporated into their food chain; hence, the essential pathways of microplastics we obtained would be helpful to assess their potential risks in an aquatic ecosystem.

4. Conclusions

In this work, Markovian predictive models were introduced to study the transport of real PE microplastic particles in open-channel flows. First, we found that travel time PDFs provide enough information to faithfully reproduce microplastic transport in both an idealized numerical open-channel flow and a more realistic real-world laboratory experiment. However, coupling travel time PDFs with strong correlation effects associated with the open-channel system is essential. Then, as part of this work, a series of Markov models were trained with such PDF data in an effort to accurately predict downstream BTCs. Among the trained three Markov models, we found that the correlated Bernoulli model (via parameter p) and correlated SMM (via a transition matrix) showed advantages in accurately predicting BTCs, which emphasizes the significance of correlation effects between successive steps. As to which correlated model is better, the choice should be made according to the specific hydrodynamic conditions, although given the much more parsimonious nature of the Bernoulli model, this would most likely be our recommendation across the board. Furthermore, the computational cost of the Markov models is orders of magnitude less than that of something like a full DNS. As such, the correlated Markov models are computationally efficient tools which can help us understand microplastic transport in open-channel flow systems, not just for idealized conditions, but also in reality. This will provide a reliable foundation for researchers to build on, especially when dealing with rising concerns of microplastic associated transport of other pollutants.

Data Availability Statement

The code used to establish the three Markov models is made public at <https://zenodo.org/badge/latestdoi/434471939>.

References

- Aquino, T., & Borgne, T. L. (2021). The diffusing-velocity random walk: A spatial-Markov formulation of heterogeneous advection and diffusion. *Journal of Fluid Mechanics*, 910, A12. <https://doi.org/10.1017/jfm.2020.957>
- Arthur, C., Baker, J., & Bamford, H. (2008). International research workshop on the occurrence, effects, and fate of microplastic marine debris. In *Conference proceedings. Sept* (pp. 9–11).
- Aubeneau, A., Hanrahan, B., Bolster, D., & Tank, J. L. (2014). Substrate size and heterogeneity control anomalous transport in small streams. *Geophysical Research Letters*, 41(23), 8335–8341. <https://doi.org/10.1002/2014gl061838>
- Berkowitz, B., Cortis, A., Dentz, M., & Scher, H. (2006). Modeling non-Fickian transport in geological formations as a continuous time random walk. *Reviews of Geophysics*, 44(2). <https://doi.org/10.1029/2005rg000178>
- Besseling, E., Quik, J. T., Sun, M., & Koelmans, A. A. (2017). Fate of nano- and microplastic in freshwater systems: A modeling study. *Environmental Pollution*, 220, 540–548. <https://doi.org/10.1016/j.envpol.2016.10.001>
- Bianchi Janetti, E., Sherman, T., Guédon, G. R., Bolster, D., & Porta, G. M. (2020). Upscaling of solute plumes in periodic porous media through a trajectory-based spatial Markov model. *Water Resources Research*, 56(12), e2020WR028408. <https://doi.org/10.1029/2020wr028408>
- Bolster, D., Méheust, Y., Borgne, T. L., Bouquain, J., & Davy, P. (2014). Modeling preasymptotic transport in flows with significant inertial and trapping effects—The importance of velocity correlations and a spatial Markov model. *Advances in Water Resources*, 70, 89–103. <https://doi.org/10.1016/j.advwatres.2014.04.014>

Acknowledgments

This work was carried out while Liming Xing was at the Department of Civil and Environmental Engineering and Earth Sciences, University of Notre Dame, as a research scholar, with the support of the China Scholarship Council (No. 201906040139). The financial support of the National Key R&D Program (2018YFC1406401) is gratefully acknowledged. DB and TS also acknowledge funding support from the National Science Foundation via grant EAR-2049688.

- Browne, M. A., Crump, P., Niven, S. J., Teuten, E., Tonkin, A., Galloway, T., & Thompson, R. (2011). Accumulation of microplastic on shorelines worldwide: Sources and sinks. *Environmental Science & Technology*, 45(21), 9175–9179. <https://doi.org/10.1021/es201811s>
- De Anna, P., Le Borgne, T., Dentz, M., Tartakovsky, A. M., Bolster, D., & Davy, P. (2013). Flow intermittency, dispersion, and correlated continuous time random walks in porous media. *Physical Review Letters*, 110(18), 184502. <https://doi.org/10.1103/physrevlett.110.184502>
- Dibenedetto, M. H., & Ouellette, N. T. (2018). Preferential orientation of spheroidal particles in wavy flow. *Journal of Fluid Mechanics*, 856, 850–869. <https://doi.org/10.1017/jfm.2018.738>
- Dietrich, W. E. (1982). Settling velocity of natural particles. *Water Resources Research*, 18(6), 1615–1626. <https://doi.org/10.1029/wr018i006p01615>
- Duan, J., Bolan, N., Li, Y., Ding, S., & Kirkham, M. B. (2021). Weathering of microplastics and interaction with other coexisting constituents in terrestrial and aquatic environments. *Water Research*, 196, 117011. <https://doi.org/10.1016/j.watres.2021.117011>
- Engdahl, N. B. (2018). Simulating the mobility of micro-plastics and other fiber-like objects in saturated porous media using constrained random walks. *Advances in Water Resources*, 121(Nov), 277–284. <https://doi.org/10.1016/j.advwatres.2018.08.011>
- Engdahl, N. B., & Bolster, D. (2020). Markovian transport processes in a heterogeneous, variably saturated watershed: A multi-domain spatial Markov model. *Advances in Water Resources*, 138, 103555. <https://doi.org/10.1016/j.advwatres.2020.103555>
- Geyer, R., Jambeck, J. R., & Law, K. L. (2017). Production, use, and fate of all plastics ever made. *Science Advances*, 3(7), e1700782. <https://doi.org/10.1126/sciadv.1700782>
- Gong, J., & Xie, P. (2020). Research progress in sources, analytical methods, eco-environmental effects, and control measures of microplastics. *Chemosphere*, 254, 126790. <https://doi.org/10.1016/j.chemosphere.2020.126790>
- Guo, X., Wang, X., Zhou, X., Kong, X., Tao, S., & Xing, B. (2012). Sorption of four hydrophobic organic compounds by three chemically distinct polymers: Role of chemical and physical composition. *Environmental Science & Technology*, 46(13), 7252–7259. <https://doi.org/10.1021/es301386z>
- Holzner, M., Morales, V. L., Willmann, M., & Dentz, M. (2015). Intermittent Lagrangian velocities and accelerations in three-dimensional porous medium flow. *Physical Review E*, 92(1), 013015. <https://doi.org/10.1103/physreve.92.013015>
- Hüffer, T., & Hofmann, T. (2016). Sorption of non-polar organic compounds by micro-sized plastic particles in aqueous solution. *Environmental Pollution*, 214, 194–201. <https://doi.org/10.1016/j.envpol.2016.04.018>
- Jambeck, J. R., Geyer, R., Wilcox, C., Siegler, T. R., Perryman, M., Andrady, A., et al. (2015). Plastic waste inputs from land into the ocean. *Science*, 347(6223), 768–771. <https://doi.org/10.1126/science.1260352>
- Kang, P. K., De Anna, P., Nunes, J. P., Bijeljic, B., Blunt, M. J., & Juanes, R. (2014). Pore-scale intermittent velocity structure underpinning anomalous transport through 3-D porous media. *Geophysical Research Letters*, 41(17), 6184–6190. <https://doi.org/10.1002/2014gl016475>
- Kang, P. K., Le Borgne, T., Dentz, M., Bour, O., & Juanes, R. (2015). Impact of velocity correlation and distribution on transport in fractured media: Field evidence and theoretical model. *Water Resources Research*, 51(2), 940–959. <https://doi.org/10.1002/2014wr015799>
- Kang, P. K., Lei, Q., Dentz, M., & Juanes, R. (2019). Stress-induced anomalous transport in natural fracture networks. *Water Resources Research*, 55(5), 4163–4185. <https://doi.org/10.1029/2019wr024944>
- Khatmullina, L., & Isachenko, I. (2017). Settling velocity of microplastic particles of regular shapes. *Marine Pollution Bulletin*, 114(2), 871–880. <https://doi.org/10.1016/j.marpolbul.2016.11.024>
- Koelmans, A. A., Besseling, E., & Foekema, E. M. (2014). Leaching of plastic additives to marine organisms. *Environmental Pollution*, 187, 49–54. <https://doi.org/10.1016/j.envpol.2013.12.013>
- Kowalski, N., Reichardt, A. M., & Wanik, J. (2016). Sinking rates of microplastics and potential implications of their alteration by physical, biological, and chemical factors. *Marine Pollution Bulletin*, 109(1), 310–319. <https://doi.org/10.1016/j.marpolbul.2016.05.064>
- Kumar, R. G., Strom, K. B., & Keyvani, A. (2010). Floc properties and settling velocity of San Jacinto estuary mud under variable shear and salinity conditions. *Continental Shelf Research*, 30(20), 2067–2081. <https://doi.org/10.1016/j.csr.2010.10.006>
- Le Borgne, T., Bolster, D., Dentz, M., de Anna, P., & Tartakovsky, A. (2011). Effective pore-scale dispersion upscaling with a correlated continuous time random walk approach. *Water Resources Research*, 47(12). <https://doi.org/10.1029/2011wr010457>
- Le Borgne, T., Dentz, M., & Carrera, J. (2008a). Lagrangian statistical model for transport in highly heterogeneous velocity fields. *Physical Review Letters*, 101(9), 090601. <https://doi.org/10.1103/physrevlett.101.090601>
- Le Borgne, T., Dentz, M., & Carrera, J. (2008b). Spatial Markov processes for modeling Lagrangian particle dynamics in heterogeneous porous media. *Physical Review E - Statistical, Nonlinear and Soft Matter Physics*, 78(2), 026308. <https://doi.org/10.1103/physreve.78.026308>
- Li, Y., Liu, S., Liu, M., Huang, W., Chen, K., Ding, Y., et al. (2021). Mid-level riverine outflow matters: A case of microplastic transport in the Jiulong River, China. *Frontiers in Marine Science*, 8, 712727. <https://doi.org/10.3389/fmars.2021.712727>
- Löder, M. G. J., Kuczera, M., Mintenig, S., Lorenz, C., & Gerdts, G. (2015). Focal plane array detector-based micro-Fourier-transform infrared imaging for the analysis of microplastics in environmental samples. *Environmental Chemistry*, 12(5), 563–581. <https://doi.org/10.1071/en14205>
- Morales, V. L., Dentz, M., Willmann, M., & Holzner, M. (2017). Stochastic dynamics of intermittent pore-scale particle motion in three-dimensional porous media: Experiments and theory. *Geophysical Research Letters*, 44(18), 9361–9371. <https://doi.org/10.1002/2017gl074326>
- Mughini-Gras, L., van der Plaats, R. Q. J., van der Wielen, P. W. J. J., Bauerlein, P. S., & de Roda Husman, A. M. (2021). Riverine microplastic and microbial community compositions: A field study in the Netherlands. *Water Research*, 192, 116852.
- Murphy, F., Ewins, C., Carbonnier, F., & Quinn, B. (2016). Wastewater treatment works (WTW) as a source of microplastics in the aquatic environment. *Environmental Science & Technology*, 50(11), 5800–5808. <https://doi.org/10.1021/acs.est.5b05416>
- Nel, H., & Froneman, P. (2015). A quantitative analysis of microplastic pollution along the south-eastern coastline of South Africa. *Marine Pollution Bulletin*, 101(1), 274–279. <https://doi.org/10.1016/j.marpolbul.2015.09.043>
- Park, H. J., Sherman, T., Freire, L. S., Wang, G., Bolster, D., Xian, P., et al. (2020). Predicting vertical concentration profiles in the marine atmospheric boundary layer with a Markov chain random walk model. *Journal of Geophysical Research: Atmospheres*, 125(19), e2020JD032731. <https://doi.org/10.1029/2020jd032731>
- Richter, D. H., & Sullivan, P. P. (2013). Momentum transfer in a turbulent, particle-laden Couette flow. *Physics of Fluids*, 25(5), 053304. <https://doi.org/10.1063/1.4804391>
- Sherman, T., Engdahl, N. B., Porta, G., & Bolster, D. (2020). A review of spatial Markov models for predicting pre-asymptotic and anomalous transport in porous and fractured media. *Journal of Contaminant Hydrology*, 236, 103734. <https://doi.org/10.1016/j.jconhyd.2020.103734>
- Sherman, T., Foster, A., Bolster, D., & Singha, K. (2018). Predicting downstream concentration histories from upstream data in column experiments. *Water Resources Research*, 54(11), 9684–9694. <https://doi.org/10.1029/2018wr023420>
- Sherman, T., Roche, K. R., Richter, D. H., Packman, A. I., & Bolster, D. (2019). A dual domain stochastic Lagrangian model for predicting transport in open channels with hyporheic exchange. *Advances in Water Resources*, 125, 57–67. <https://doi.org/10.1016/j.advwatres.2019.01.007>

- Sighicelli, M., Pietrelli, L., Lecce, F., Iannilli, V., Falconieri, M., Coscia, L., et al. (2018). Microplastic pollution in the surface waters of Italian Subalpine Lakes. *Environmental Pollution*, 236, 645–651. <https://doi.org/10.1016/j.envpol.2018.02.008>
- Teng, J., Zhao, J., Zhang, C., Cheng, B., Koelmans, A. A., Wu, D., et al. (2020). A systems analysis of microplastic pollution in Laizhou Bay, China. *Science of The Total Environment*, 745, 140815. <https://doi.org/10.1016/j.scitotenv.2020.140815>
- Vincent, A. E., & Hoellein, T. J. (2021). Distribution and transport of microplastic and fine particulate organic matter in urban streams. *Ecological Applications*, 31(8), e02429. <https://doi.org/10.1002/eap.2429>
- Wang, J., Qin, X., Guo, J., Jia, W., & Huang, Y. (2020). Evidence of selective enrichment of bacterial assemblages and antibiotic resistant genes by microplastics in urban rivers. *Water Research*, 183, 116113. <https://doi.org/10.1016/j.watres.2020.116113>
- Xuan, G. A., & Jwa, B. (2019). The chemical behaviors of microplastics in marine environment: A review. *Marine Pollution Bulletin*, 142, 1–14. <https://doi.org/10.1016/j.marpolbul.2019.03.019>
- Zhang, W., Zhang, S., Wang, J., Wang, Y., Mu, J., Wang, P., et al. (2017). Microplastic pollution in the surface waters of the Bohai Sea, China. *Environmental Pollution*, 231, 541–548. <https://doi.org/10.1016/j.envpol.2017.08.058>
- Zhao, S., Zhu, L., & Li, D. (2015). Microplastic in three urban estuaries, China. *Environmental Pollution*, 206, 597–604. <https://doi.org/10.1016/j.envpol.2015.08.027>